Voigt, J.R.C., et al., 2021, Linking lava morphologies to effusion rates for the 2014–2015 Holuhraun lava flow field, Iceland: Geology, https://doi.org/10.1130/G49251.1

Supporting Information for

Linking Lava Morphologies to Effusion Rates for the 2014–2015 Holuhraun Lava Flow-Field, Iceland

Joana R. C. Voigt[1], Christopher W. Hamilton[1], Gregor Steinbrügge[2], Ármann Höskuldsson[3], Ingibjörg Jónsdottir[4], and Thorvaldur Thordarson[4]

[1] *Lunar and Planetary Laboratory, University of Arizona, Tucson AZ, 85721, USA*

[2] *Department of Geophysics, Stanford University, Stanford, California, USA*

[3] *Faculty of Earth Sciences, University of Iceland, Reykjavík, Iceland*

[4] *Nordic Volcanological Centre, Institute of Earth Sciences, University of Iceland, Reykjavík, Iceland*

Supplementary Material

Previously Established Links between Emplacement Conditions and Lava Types

Macdonald (1953) and Williams and McBirney (1979) asserted that the main factors controlling the development of different subaerial lava morphologies are related to the physical properties of the lava. These factors include composition, temperature, water content, vesicularity, crystallinity, and melt polymerization—which together control lava viscosity. However, shear strain rate is also an important factor, with low shear strain rates favoring the development of pāhoehoe flows with stable surfaces, and high shear strain rates favoring the disruption of lava surfaces and the development of ‘a‘ā flows (Hon et al., 2003; Rowland and Walker, 1990). Shear strain rate can be affected by global parameters, such as planetary mass

and gravitational acceleration, as well as mass flux rates at the vent (i.e., the instantaneous effusion rate of lava entering into the lava transport system, and local factors). Local factors affecting volumetric fluxes through specific sections of the lava transport system include lobe thickness and underlying slope (Glaze et al., 2014; Rowland and Walker, 1990); pathway geometry (Lev and James, 2014) and branch factor (Dietterich and Cashman, 2014); substrate roughness (Hamilton et al., 2013; Rumpf et al., 2018); the formation and release of blockages (Harris et al., 2009; James et al., 2012; Patrick and Orr, 2012), and other static and dynamic effects (Glaze et al., 2014). Other factors being equal, high shear strain rates tends to favor the formation of disrupted crust and low shear strain rates favors the development of a stable crust (Hon et al., 2003; Rowland and Walker, 1990). Other parameters that can affect volumetric fluxes and shear strain rates are related to the eruption source conditions, such as the conduit shape and size, which will affect the instantaneous effusion rate entering into the lava transport system at the vent. The total duration of lava supply can also exert a large control on lava flow morphologies by control how the lava pathways evolve through time (e.g., Hon et al., 2003; Peterson and Tilling, 1980).

In general, lava products can be linked to their emplacement dynamics (Hon et al., 2003; Peterson and Tilling, 1980; Thordarson and Höskuldsson, 2008; Thordarson and Larsen, 2007; Thordarson and Self, 1998). For example, pāhoehoe flows are a typically product from Hawaiian styles of eruptive activity and at relatively low local effusion rates are mainly composed of interconnected and endogenously-fed lobes that supply lava to the flow front via thermally insulated preferred pathways (e.g., lava tubes) (Keszthelyi, 1995; Self et al., 1998; Thordarson and Self, 1998). In contrast, ʻaʻā lava flows are commonly associated with higher effusion rate Hawaiian eruptions and Strombolian eruptions, which can both feed lava through open-channel

systems at high effusion rates (Rowland and Walker, 1990). Flood lavas and flood basalt eruptions can produce both end-members lava types but can also exhibit a spectrum of transitional lavas or subtypes (e.g., Keszthelyi and Self, 1998; Keszthelyi et al., 2004; Self et al., 1998; Thordarson and Höskuldsson, 2008; Thordarson and Self, 1998). These transitional lavas can result from pulsating lava effusion conditions at the vent, or the local damming and release of lava that is temporarily stored along a segment of the lava pathway system, resulting in local surges or shocks that can disrupt stable lava crusts into platy, slabby, and rubbly lavas (Hamilton, 2019).

Parameters such as emplacement sequence (e.g., the chronological emplacement of different flow units), pre-eruption topography, and effusion rates are hard to derive from the geologic record. Theoretical models have investigated the influence of thermo-rheological properties of the lava and terrain parameters such as pre-eruption slopes on the development of channelized flows and lava disruption (e.g., Chevrel et al., 2013; Glaze et al., 2014). Experimental work further suggested that effusion rates affect the emplacement dynamics and morphology (e.g., Fink and Griffiths, 1992). Rader et al. (2017) have shown that unsteady effusion rates can affect lava inflation processes resulting in different geomorphological characteristics. However, to date no studies have systematically investigated the potential link between lava effusion rates and surficial lava characteristics on a recent eruption that was dominated by transitional lavas.

Data and Methods

The chronological map is based on field-based Global Positioning System (GPS) measurements as well as airborne radar measurements (see Pedersen et al. (2017) for a detailed description). Additionally, imaging and elevation data were obtained by a radar onboard the TerraSAR-X and TanDEM-X twin satellites, which monitored the Holuhraun eruption site (Dirscherl and Rossi, 2018). In 2014, data were acquired on September 4th, 9th, 15th; October 7th, 18th, 29th; December 1st, 6th; and in 2015, data were collected on January 19th; February 10th, 26th, and 27th. These data were analyzed to reconstruct the growth of the lava flow-field (Figure 1A). The twin satellites are operated by the German Aerospace Center (DLR). Pre-eruption datasets, which are valuable for evaluating the terrain context prior the eruption, include two Loftmyndir ehf. orthomosaics from 2003 and 2013 and its derived digital elevation model. These datasets both have resolutions of 50 cm/pixel and were combined into a single orthomosaic basemap. The UltraCam-Xp orthomoasic with a resolution of 20 cm/pixel provided post-eruption context information (Münzer et al., 2016). These data products were imported into the Esri-software ArcGIS version 10.7.1 to generate the chronological map by manually digitizing the evolution of the flow margin with each time step. Additionally, a pre-eruption map was developed to qualitatively evaluate possible influences of the pre-eruption terrain on the flow-field (Figure S1). Both maps were digitized at a scale of 1:1,500.

Two independently derived Time Averaged Discharge Rate (TADR) datasets were analyzed for this study. The TADRs presented by Coppola et al. (2017) were derived from thermal infrared data from the MOderate Resolution Imaging Spectroradiometer (MODIS; see Coppola et al. (2019) and references therein); and the second TADR dataset by Bonny et al. (2018) combines MODIS infrared data with field measurements of the flows volume. Both TADR datasets generally exhibit similar patterns; but the magnitudes of the absolute TADR

values vary. The main reasons for these differences stem from the flow thickness normalizations and assumed input temperatures used in the models (Bonny et al., 2018).

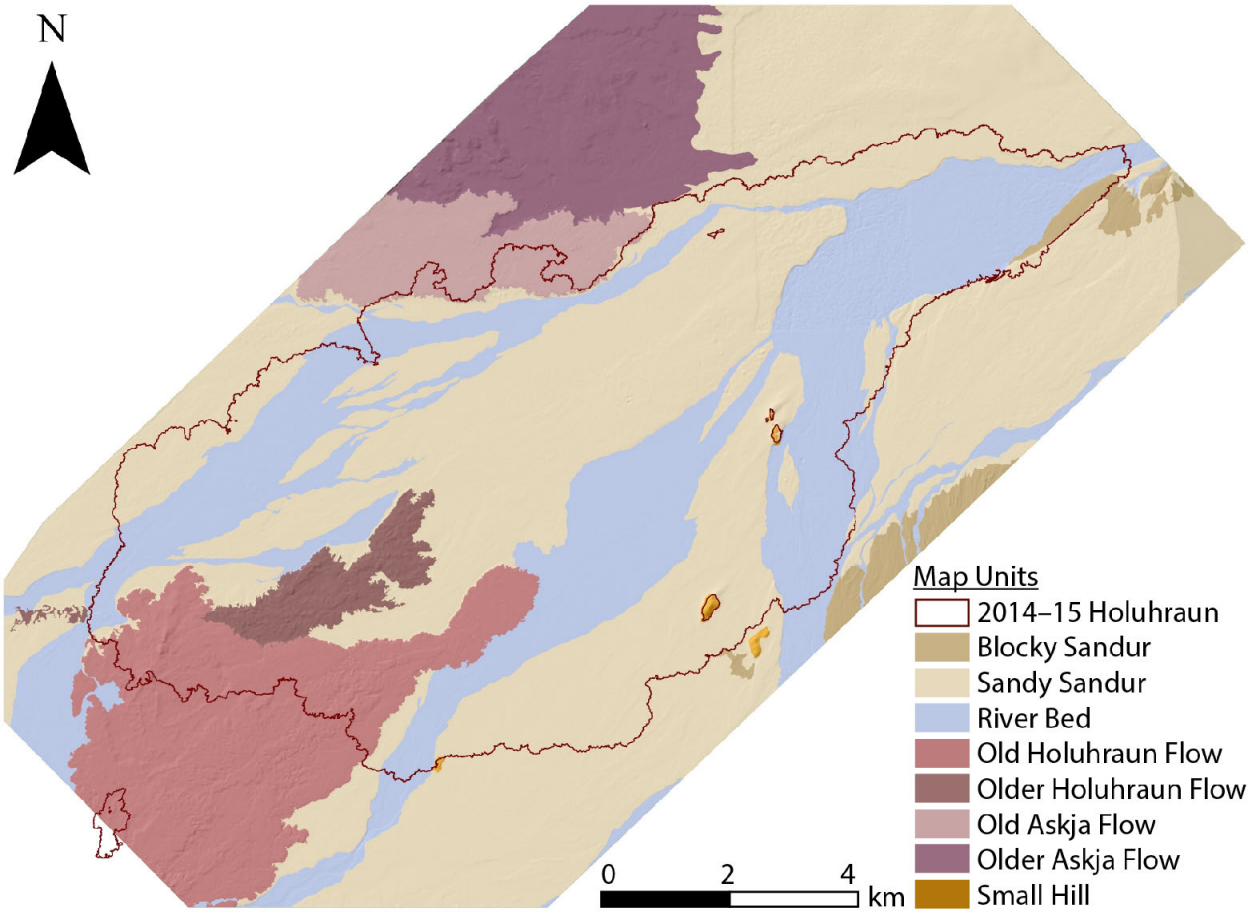

Figure S1. Pre-eruption map illustrating the main geological units. Map is overlain on a hillshade basemap (Loftmyndir ehf.) and map was created based on a digitizing scale of 1:1500. The red tones indicate older Holuhraun flows and the purple tones older Askja lava flows. The blue polygon marks the active riverbed from Jökulsá á Fjöllum river prior the eruption that carved into the Dyngjusandur glacial outwash plain marked with yellow tones including blocky and sandy terrain as well as small hills. The figure is centered at 16°40’51 W and 64°53’13 N.

Correlation

To perform the correlation between the facies and the effusion rate, we start with a time series of TADRs and a time series of emplaced areas A_t, where t designates the chronological unit. For each chronological unit the emplaced area divides further into subareas $a_{t,f}$, where f designates the individual facies such that $A_t = \Sigma_f(a_{t,f})$. We can further compute the total area of a facies A_f emplaced over the total eruption $A_f = \Sigma_t(a_{t,f})$ and the total area of the entire lava flow $A = \Sigma_f \Sigma_t(a_{t,f})$.

For the normalization used in the main part we compute the area emplaced by one facies per chronological unit $a_{t,f}$ divided by the area of all facies emplaced during the same chronological unit A_t. For normalizing using the total emplaced area of a facies we have to account for the inhomogeneous spacing of the chronological units. Therefore, we first divide $a_{t,f}$ by the number of days within the chronological unit of index $t(d_t)$. Only afterwards we divide by A_f.

Facies emplacement was therefore normalized by the total area of all facies emplaced per day as:

$$F_t = a_{t,f}/A_t, \qquad \text{[Eq. 1]}$$

with the facies emplacement normalized by the total area covered by each facies over the entire eruption as:

$$F_f = a_{tf}/(d_t A_t). \qquad \text{[Eq. 2]}$$

These two factors cannot directly be correlated with the TADR since the time base is different in the TADR data. To compensate for this, we linearly interpolated the data with a

timestep of 0.025 days before correlation. For the variance we utilized a running window in which the variance is computed. The width of this window is 11 days.

Results (normalized by entire eruption)

Since it is obvious that the total emplaced area per day correlates with the effusion rate, some form of normalization is necessary. Two metrics are conceivable here: (1) computing the area of an individual facies emplaced per chronological unit normalized by the total area of this facies emplaced over the entire eruption; or (2) computing by normalizing the area of an individual facies emplaced per chronological unit normalized by the total area of all facies emplaced this day (see main text). Emplacement over the entire eruption is discussed in less detail because if lava is erupted onto the surface, it needs to be correlated with the lava facies. Nonetheless, the information is important as additional input because it reveals how much areal extension specific chronological units have (Figure S3 and 4).

The strongest correlation with a Spearman correlation coefficient of 82% occurs for the Rubbly facies with the TADR and 78% with the variance when analyzed over the entire eruption (Coppola et al., 2017).

Table S1. Spearman correlation coefficient with a color code showing the degree of correlation: 0.00–0.19 = very weak; 0.20–0.39 = weak; 0.40–0.59 = moderate (yellow); 0.60–0.79 = strong (light green); 0.80–1.0 = very strong (dark green). [1]TADR from Coppola et al. (2017) and [2]TADR from Bonny et al. (2018).

Facies	Correlation Coefficient							
	Over entire Eruption				Per Day			
	TADR[1]	Var. of TADR[1]	TADR[2]	Var. of TADR[2]	TADR[1]	Var. of TADR[1]	TADR[2]	Var. of TADR[2]
Rubbly	0.82	0.78	0.76	0.70	0.71	0.61	0.64	0.48
Spiny	−0.61	−0.52	−0.62	−0.47	−0.66	−0.61	−0.63	−0.58
Undiffer.	0.56	0.65	0.65	0.67	0.54	0.58	0.65	0.64

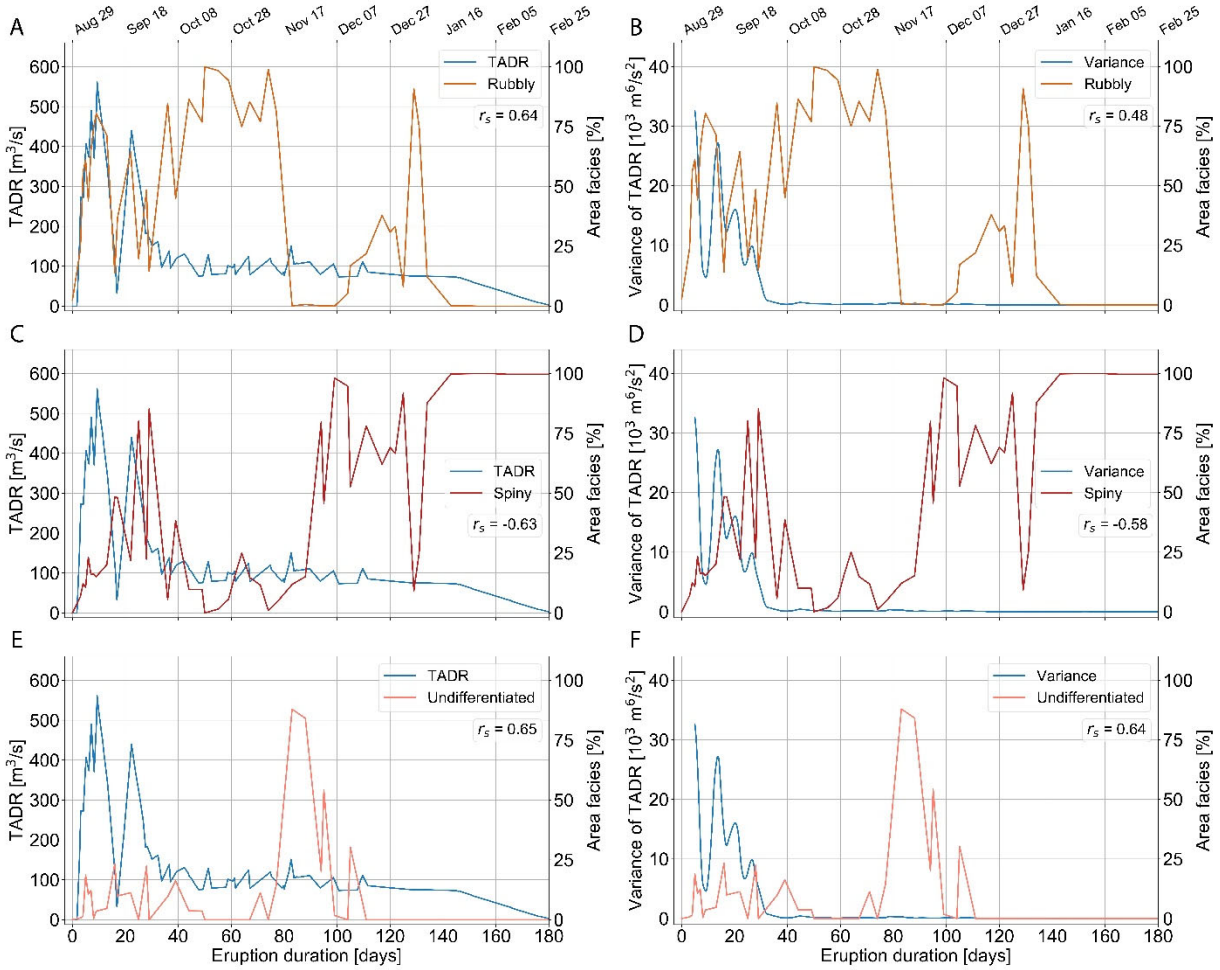

Figure S2. TADR and its derived variance from Bonny et al. (2018) and the main facies emplaced per day shown in percentage: (A) and (B) *rubbly*; (C) and (D) *spiny*; and (E) and (F) *undifferentiated rubbly–spiny* facies.

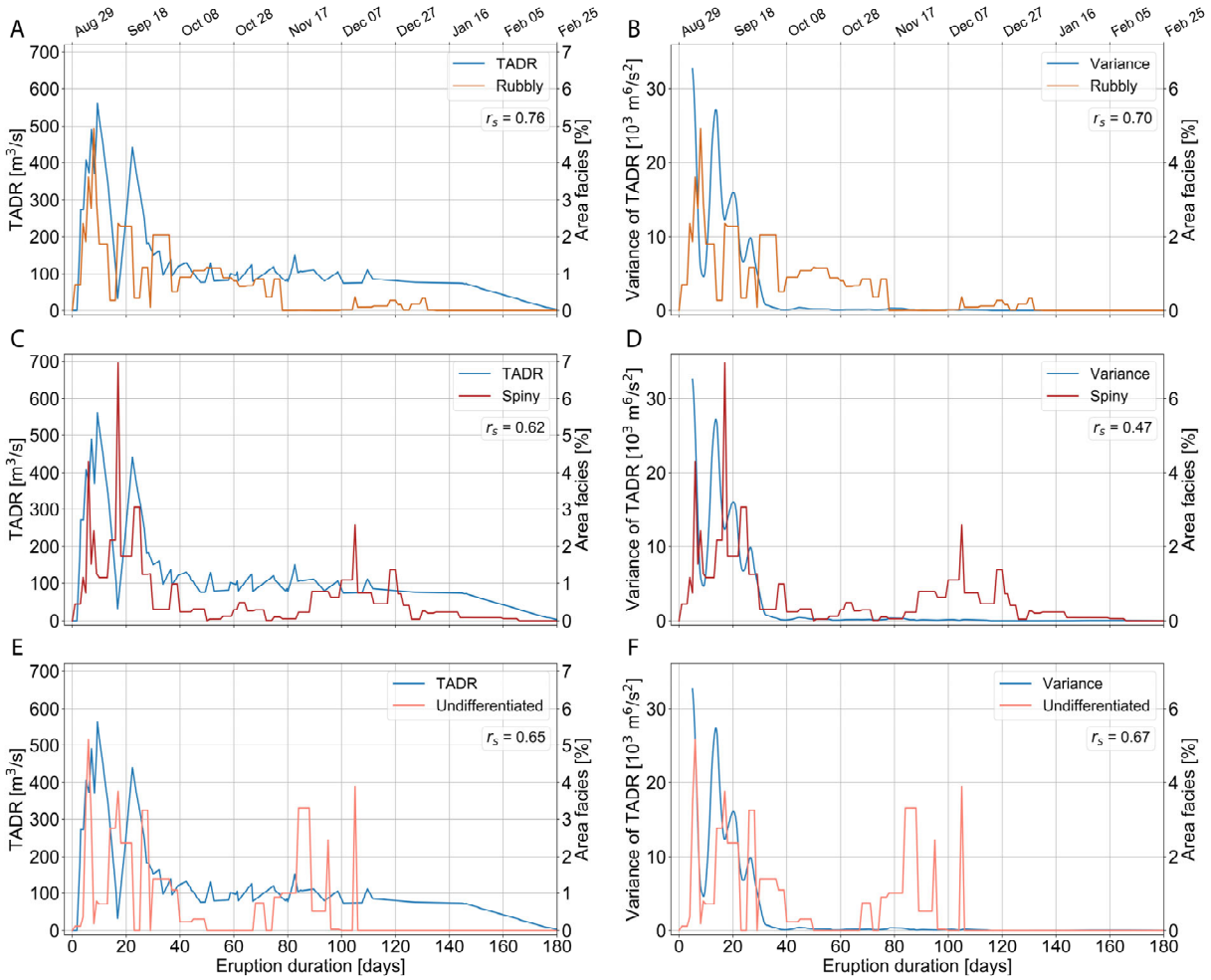

Figure S3. TADR and its derived variance from Bonny et al. (2018) and the main facies emplaced normalized by entire eruption shown in percentage: (A) and (B) *rubbly*; (C) and (D) *spiny*; and (E) and (F) *undifferentiated rubbly–spiny* facies.

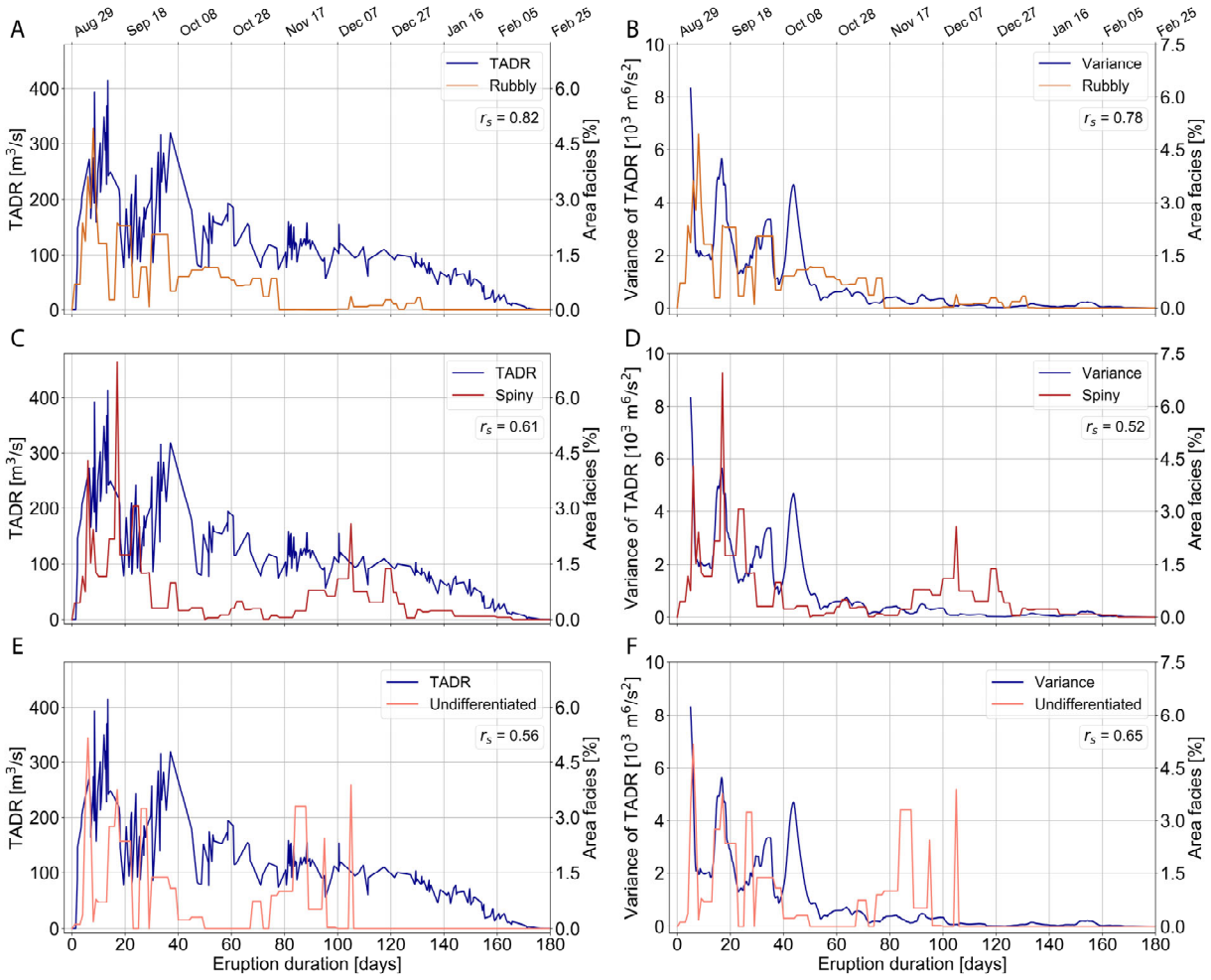

Figure S4. TADR and its derived variance from Coppola et al. (2017) and the main facies emplaced normalized by entire eruption shown in percentage: (A) and (B) *rubbly*; (C) and (D) *spiny*; and (E) and (F) *undifferentiated rubbly–spiny* facies.

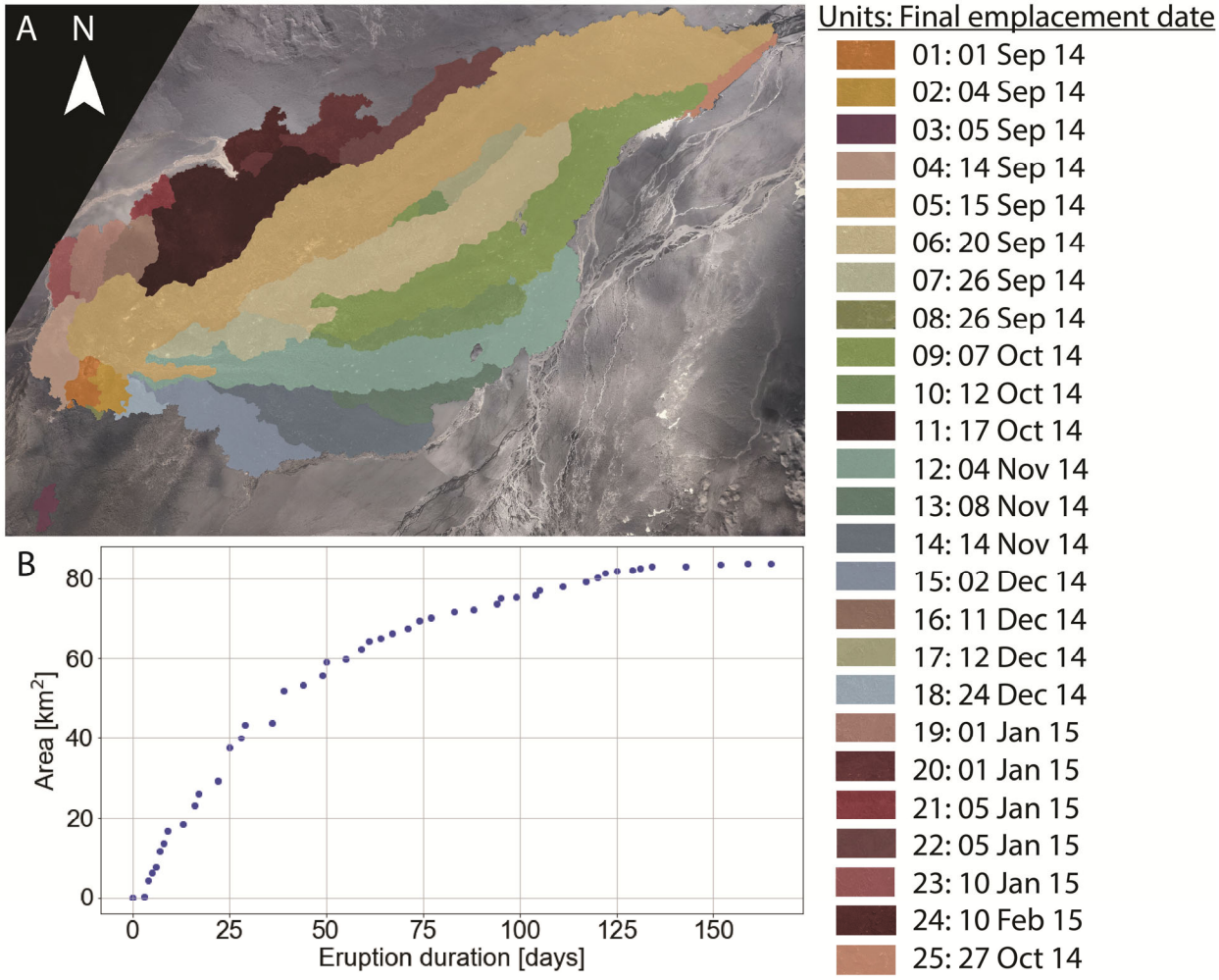

Figure S5. (A) Flow unit map of the Holuhraun lava flow-field with the final emplacement date noted in the legend. (B) Cumulative areal growth of the lava flow-field plotted over the course of the eruption in days.

Limitations

Whereas the correlation of facies emplacement with the variance shows very similar trends as the TADR, the somewhat lower correlation values of the *rubbly* and *spiny* facies with the variance can be caused due the TADR measurements not having the necessary temporal

resolution to capture individual surges and disruption events. Voigt et al. (2021) calculated that some lava surfaces were disrupted after approximately 6 hours of stable growth to form rubbly facies. With a measurement frequency of once every 24 hours by Bonny et al. (2018), a disruption time scale on the order of hours is not captured.

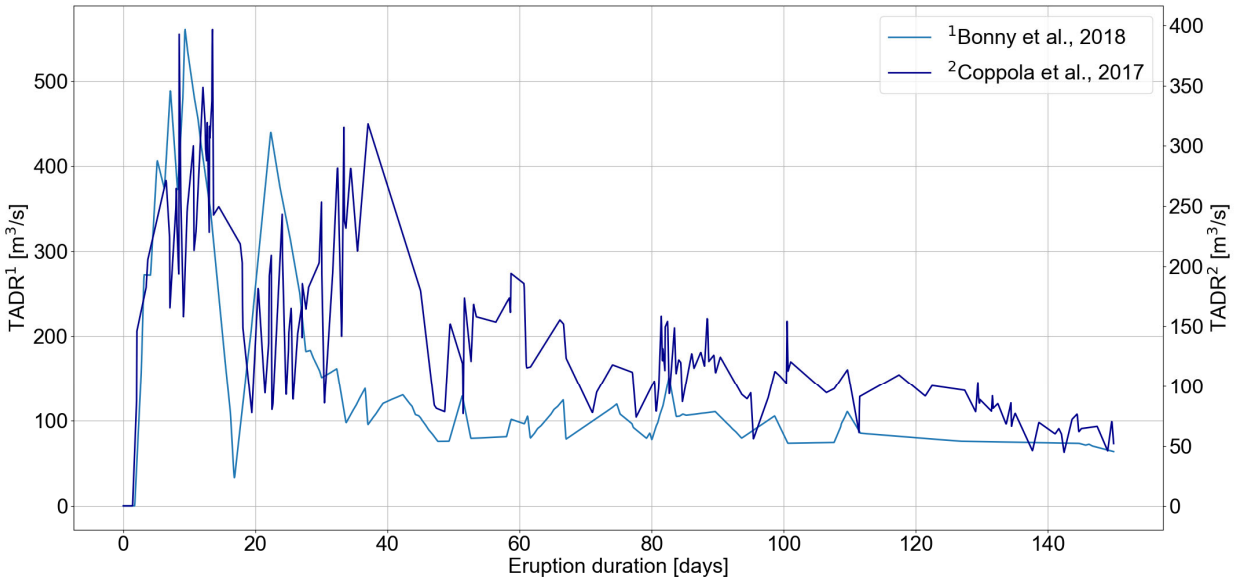

Figure S6. Plot shows the two TADRs from Bonny et al. (2018) in light blue (with the corresponding axis on the left) and from Coppola et al. (2017) in dark blue (right axis). Note that the TADR in light blue is derived from ground-based observations and the dark blue is satellite derived. The Spearman correlation coefficient of these two datasets is 0.72. Please note the two y- axes and thus the different absolute values.

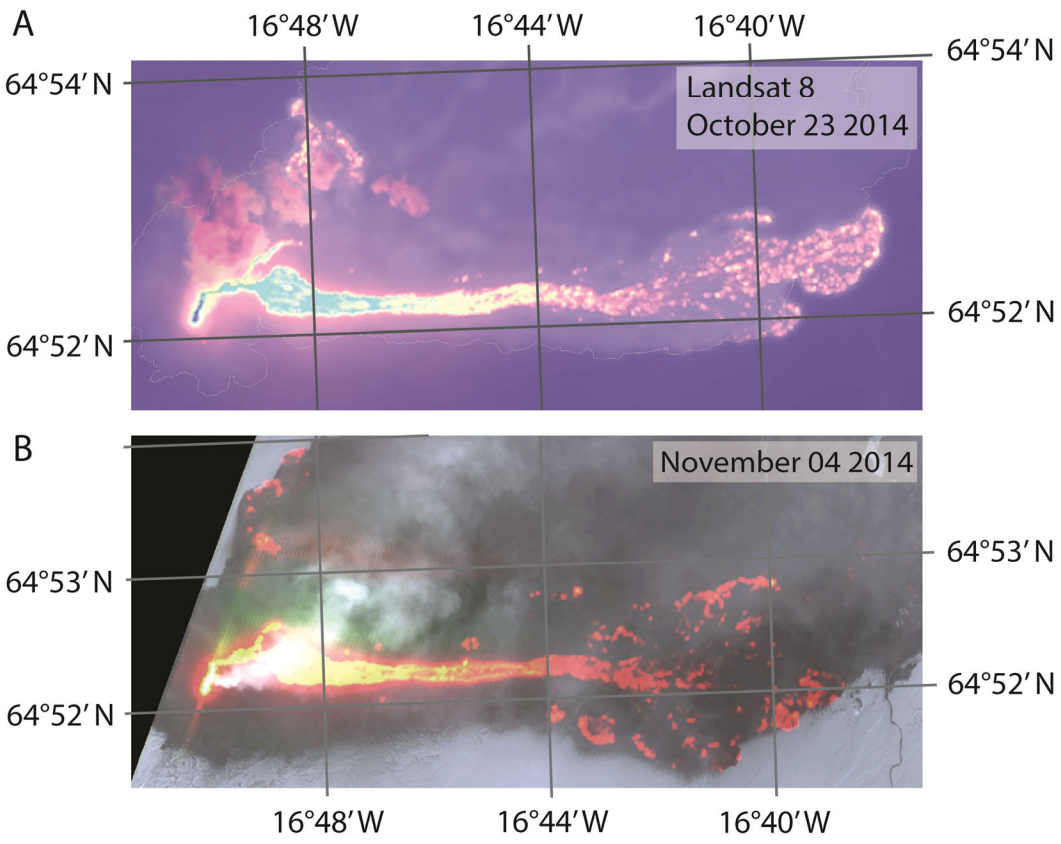

Figure S6. (A) Lava pond observed from Landsat on October 23rd 2014 and (B) on November 4th 2014. The pond acts as a major distributor of lava during this phase of the eruption and is feeding large rubbly pāhoehoe units.

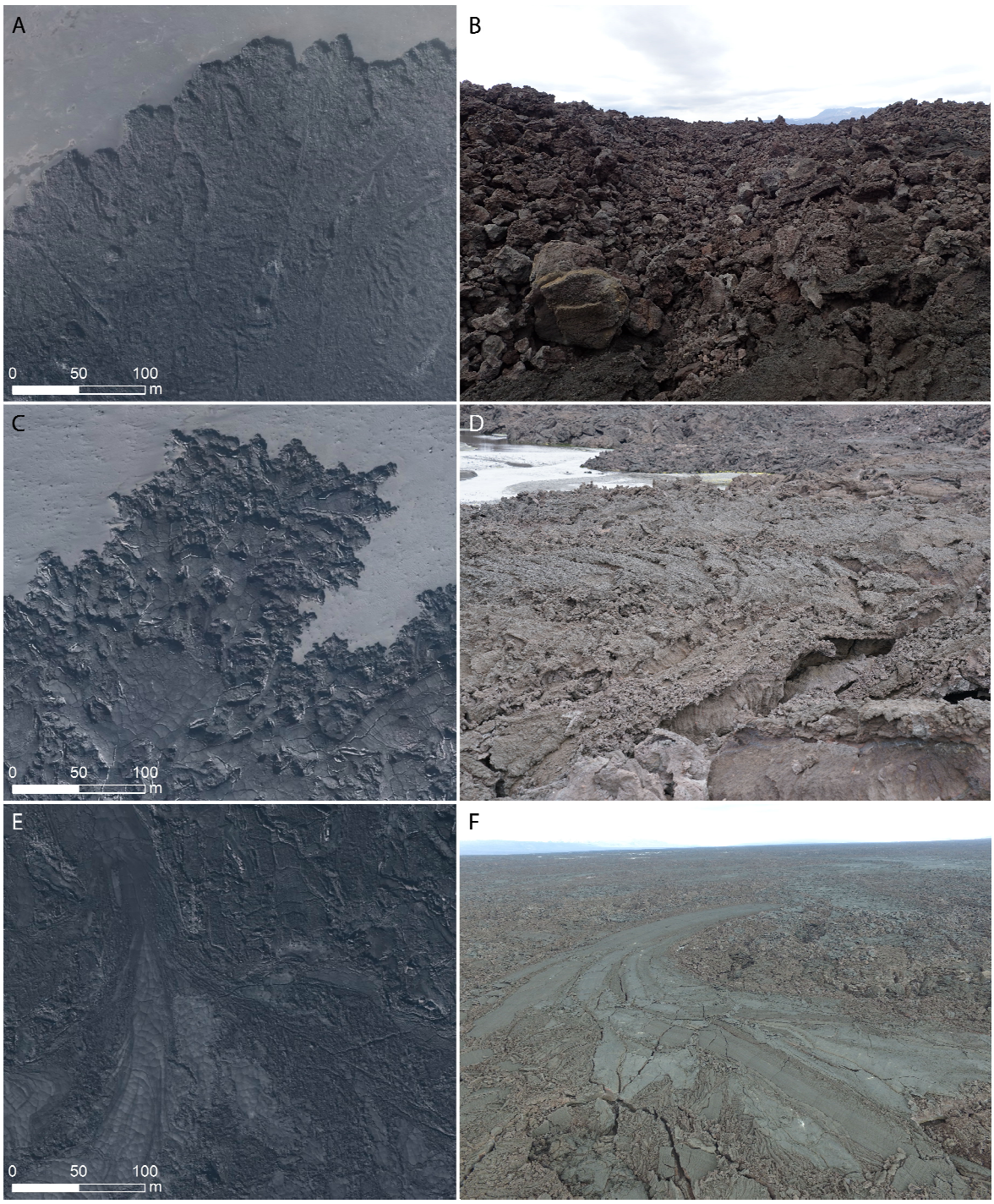

Figure S7. (A) and (B) are examples for the *rubbly* facies, (C) and (D) show *spiny* facies examples, and (E) and (F) are examples for the *undifferentiated rubbly–spiny* facies. Left panels

show remote-sensing data from the UltraCam-Hp basemap and right panels show field images, (F) is a drone image.

Overprinting

Facies such as the *vent-proximal edifice* and the *channel interior* were repeatedly modified after their initial emplacement and are thus not representative of primary TADR controls for this study. Similarly, the *shelly* facies is primarily interpreted to be formed overbank flows (e.g., in close association with the channel's activity) and thus are less likely to be formed by the initial emplacement. Further, a few lava flows and lobes within the pāhoehoe facies can be tracked back to the smaller cones that were active during the very early stage of the eruption rather than Baugur.

References

Bonny, E., Thordarson, T., Wright, R., Höskuldsson, A. and Jónsdóttir, I., 2018. The Volume of Lava Erupted During the 2014 to 2015 Eruption at Holuhraun, Iceland: A Comparison Between Satellite- and Ground-Based Measurements. Journal of Geophysical Research: Solid Earth, 123(7): 5412–5426.

Coppola, D., Barsotti, S., Cigolini, C., Laiolo, M., Pfeffer, M.A. and Ripepe, M., 2019. Monitoring the time-averaged discharge rates, volumes and emplacement style of large lava flows by using MIROVA system: the case of the 2014-2015 eruption at Holuhraun (Iceland). Annals of Geophysics, 62(2).

Coppola, D., Ripepe, M., Laiolo, M. and Cigolini, C., 2017. Modelling satellite-derived magma discharge to explain caldera collapse. Geology, 45(6): 523–526.

Dietterich, H.R. and Cashman, K.V., 2014. Channel networks within lava flows: Formation, evolution, and implications for flow behavior. Journal of Geophysical Research: Earth Surface, 119(8): 1704-1724.

Glaze, L.S., Baloga, S.M., Fagents, S.A. and Wright, R., 2014. The influence of slope breaks on lava flow surface disruption. Journal of Geophysical Research: Solid Earth, 119(3): 1837-1850.

Hamilton, C.W., 2019. “Fill and spill” lava flow emplacement: Implications for understanding planetary flood basalt eruptions. , Marshall Space Flight Center, Faculty Fellowship Program, NF Six and R Damiani (Eds.), NASA/TM—2019–220139, 47–56.

Hamilton, C.W., Glaze, L.S., James, M.R. and Baloga, S.M., 2013. Topographic and stochastic influences on pāhoehoe lava lobe emplacement. Bulletin of Volcanology, 75(11): 756.

Harris, A.J.L., Favalli, M., Mazzarini, F. and Hamilton, C.W., 2009. Construction dynamics of a lava channel. Bulletin of Volcanology, 71(4): 459.

Hon, K., Gansecki, C. and Kauahikaua, J., 2003. The Transition from ‘A‘ä to Pähoehoe Crust on Flows Emplaced During the Pu‘u ‘Ö‘ö-Küpaianaha Eruption. U.S. Geological Survey Professional Paper 1676: 89–104.

James, M.R., Applegarth, L.J. and Pinkerton, H., 2012. Lava channel roofing, overflows, breaches and switching: insights from the 2008–2009 eruption of Mt. Etna. Bulletin of Volcanology, 74(1): 107-117.

Keszthelyi, L., 1995. A preliminary thermal budget for lava tubes on the Earth and planets. Journal of Geophysical Research: Solid Earth, 100(B10): 20411-20420.

Keszthelyi, L. and Self, S., 1998. Some physical requirements for the emplacement of long basaltic lava flows. Journal of Geophysical Research: Solid Earth, 103(B11): 27447-27464.

Keszthelyi, L., Thordarson, T., McEwen, A., Haack, H., Guilbaud, M.-N., Self, S. and Rossi, M.J., 2004. Icelandic analogs to Martian flood lavas. Geochemistry, Geophysics, Geosystems, 5(11).

Lev, E. and James, M.R., 2014. The influence of cross-sectional channel geometry on rheology and flux estimates for active lava flows. Bulletin of Volcanology, 76(7): 829.

Macdonald, G.A., 1953. Pahoehoe, aa, and block lava. American Journal of Science, 251(3): 169–191.

Münzer, Ü., Jaenicke, J., Eineder, M., Minet, C., Braun, L., Mayer, C., Siegert, F. and Franke, J., 2016. Anwendung neuer Methoden mit hochauflösenden Fernerkundungs-daten

(TerraSAR-X, TanDEM-X, RapidEye, UltraCam, HRSC) zur Früherkennung subglazialer Vulkanausbrüche auf Island. Final Report, pp. 1–85.

Patrick, M.R. and Orr, T.R., 2012. Rootless shield and perched lava pond collapses at Kīlauea Volcano, Hawai'i. Bulletin of Volcanology, 74(1): 67-78.

Pedersen, G.B.M., Höskuldsson, A., Dürig, T., Thordarson, T., Jónsdóttir, I., Riishuus, M.S., Óskarsson, B.V., Dumont, S., Magnusson, E., Gudmundsson, M.T., Sigmundsson, F., Drouin, V.J.P.B., Gallagher, C., Askew, R., Gudnason, J., Moreland, W.M., Nikkola, P., Reynolds, H.I. and Schmith, J., 2017. Lava field evolution and emplacement dynamics of the 2014–2015 basaltic fissure eruption at Holuhraun, Iceland. Journal of Volcanology and Geothermal Research, 340: 155-169.

Peterson, D.W. and Tilling, R.I., 1980. Transition of basaltic lava from pahoehoe to aa, Kilauea Volcano, Hawaii: Field observations and key factors. Journal of Volcanology and Geothermal Research, 7(3): 271-293.

Rowland, S.K. and Walker, G.P.L., 1990. Pahoehoe and aa in Hawaii: volumetric flow rate controls the lava structure. Bulletin of Volcanology, 52(8): 615-628.

Rumpf, M.E., Lev, E. and Wysocki, R., 2018. The influence of topographic roughness on lava flow emplacement. Bulletin of Volcanology, 80(7): 63.

Self, S., Keszthelyi, L. and Thordarson, T., 1998. The Importance of Pāhoehoe. Annual Review of Earth and Planetary Sciences, 26(1): 81–110.

Thordarson, T. and Höskuldsson, Á., 2008. Postglacial volcanism in Iceland, PostglacialVI.

Thordarson, T. and Larsen, G., 2007. Volcanism in Iceland in historical time: Volcano types, eruption styles and eruptive history. Journal of Geodynamics, 43(1): 118–152.

Thordarson, T. and Self, S., 1998. The Roza Member, Columbia River Basalt Group: A gigantic pahoehoe lava flow field formed by endogenous processes? Journal of Geophysical Research: Solid Earth, 103(B11): 27411–27445.

Williams, H. and McBirney, A.R., 1979. Volcanology. Freeman, Cooper.